ECS Transactions, 75 (14) 289-300 (2016)
10.1149/07514.0289ecst ©The Electrochemical Society

Accelerated Degradation of Polymer Electrolyte Membrane Fuel Cell Gas Diffusion Layers: Performance Degradation and Steady State Liquid Water Distributions with in Operando Synchrotron X-ray Radiography

Hang Liu[a], Michael G. George[a], Nan Ge[a], Rupak Banerjee[a], Stephane Chevalier[a], Jongmin Lee[a], Pranay Shrestha[a], Daniel Muirhead[a], James Hinebaugh[a], Roswitha Zeis[b], Matthias Messerschmidt[c], Joachim Scholta[c], and Aimy Bazylak[a]*

[a] Thermofluids for Energy and Advanced Materials Laboratory, Department of Mechanical & Industrial Engineering, Institute for Sustainable Energy, Faculty of Applied Science and Engineering, University of Toronto, Toronto, Ontario, Canada
[b] Karlsruhe Institute of Technology, Helmholtz Institute Ulm, Ulm, Baden-Württemberg, Germany
[c] Zentrum für Sonnenenergie- und Wasserstoff-Forschung Baden-Württemberg, Ulm, Baden-Württemberg, Germany

As-received pristine gas diffusion layers (GDLs) were degraded through an accelerated artificial aging process by immersion into a 35% solution of H_2O_2 at 90°C for 12 hours. Polarization curves were obtained while synchrotron X-ray radiography was performed to investigate the effect of ageing on liquid water transport behavior. Peak output power density of the fuel cell composed of the aged GDL reached only 76% of that of the fuel cell composed of the pristine GDL. This performance degradation was attributed to an increase in mass transport resistance associated with liquid water accumulation at the aged GDL and flow field channel interface. The aged GDLs showed more liquid water accumulation at the microporous layer (MPL)/carbon substrate interface and carbon substrate regions than pristine GDLs at low current density operation. A fully developed water profile was established at lower current density for the aged GDLs compared to pristine GDLs.

Introduction

To date, there have been many studies dedicated to gas diffusion layer (GDL) degradation effects on the polymer electrolyte membrane (PEM) fuel cell (1-19). Hiramitsu et al. (1) operated a cell at 0.3 A/cm^2 for 10,000 hours to evaluate the impact of GDL degradation and attributed performance degradation to a reduction in gas diffusivity, which was particularly degraded in the GDL as compared to the catalyst layer (CL). Cho et al. (2) analysed the transient voltage response of an aged GDL by imposing a sudden step change in the current. They reported localized reductions of hydrophobicity in the aged GDL and GDL flooding, connecting performance losses to this degradation of hydrophobicity. Lee et al. (6) also reported the separation of PTFE from carbon fibers during repetitive freeze-thaw cycles of a fuel cell. Wu et al. (13) conducted an accelerated ageing process with a combination of elevated cell temperature and flow rate conditions. They reported a noticeable decrease in electrical resistivity and hydrophobic properties

for aged GDLs. Kandlikar et al. (16) also reported the reduction in hydrophobicity of degraded GDLs. While the above mentioned works have been instrumental in identifying the dramatic impact that degradation can have on GDL material properties and performance in a fuel cell, further work is still required to determine how GDL ageing impacts the in operando liquid water transport behaviour.

The production of hydrogen peroxide (H_2O_2) is considered to be a major degradation mechanism in the operation of PEM fuel cells (20-24). The primary mechanism of H_2O_2 degradation is through the potential corrosion of PTFE coatings and carbon fibers or particles in fuel cell materials. Das et al. (19) simulated ageing by boiling commercially available GDLs in boiling 30% H_2O_2 solution for 7 hours. Aged GDLs presented higher interfacial water adhesion forces on the surface compared to pristine samples via a sliding-angle measurement resulting in increased interfacial water accumulation. Arlt et al. (18) artificially aged GDLs by immersing Freudenberg H2315 GDLs into a solution of 30% H_2O_2 at 90°C and reported increased water content in aged GDLs.

In operando visualizations of liquid water in PEM fuel cells have provided new insights into the behaviour of liquid water inside the GDL. Specifically, synchrotron X-ray radiographic imaging has been demonstrated as a powerful tool for providing high spatial and temporal resolutions (up to 3 μm at 5 seconds per frame (25)). Several groups have successfully proved the feasibility of synchrotron X-ray imaging for investigating multiphase flow behavior in an operating fuel cell (18, 25-46). Further investigation using synchrotron based visualisation techniques is needed to determine the impact of ageing on the spatial distribution of liquid water in the GDL.

In this paper, as-received pristine GDLs were artificially aged through an accelerated process involving the immersion of the GDL into a heated solution of H_2O_2. Pristine and artificially aged GDLs were subsequently assembled into customized fuel cells for performance testing and synchrotron based X-ray radiographic imaging. In operando liquid water visualizations were obtained for a range of current densities. The spatial distributions of liquid water in the pristine and aged GDLs were compared within the GDL to determine the effect of ageing on localized liquid water transport behavior.

Methodology

Gas diffusion layer artificial ageing process

Commercially available, PTFE-treated carbon paper SGL 29BC GDLs (Sigracet, Ion Power), including a hydrophobic microporous layer (MPL), were aged and evaluated in custom PEM fuel cell. As-received pristine GDLs were immersed into a 35% H_2O_2 solution at 90°C for 12 hours in-house in order to perform the accelerated artificial ageing process. The aged GDLs were rinsed in distilled water for 24 hours to remove the residual H_2O_2 solution and then dried at 80°C in a vacuum oven (Heraeus Instrument, Hanau, Germany) for 3 hours.

Fuel cell hardware

A custom fuel cell with an active area of 0.68 cm^2(0.8 cm × 0.85 cm) was designed for in situ synchrotron X-ray radiography studies. Both the anode and cathode sides were assembled according to the standard configuration of the end plate, current collector, and graphite flow field for a PEM fuel cell. The commercial membrane of the cell was selected as a thin polymer electrolyte membrane (Nafion HP, DuPont) to minimize the impact of membrane swelling on material movement in the obtained X-ray images radiographs. A platinum loading of 0.3 mg/cm^2 was applied on both the anode and cathode sides of the membrane. Identical parallel channels for the anode and cathode flow fields were machined with repeating nominal channel and rib widths of 0.5 mm and nominal channel depths of 0.5 mm. The operating temperature was regulated by the circulation of heated water through the end plates.

To evaluate the aged GDLs, the degraded materials were used for the anode and cathode gas diffusion layers of an operating fuel cell. A reference fuel cell was assembled using and as-received pristine GDLs produced from the same lot. Both fuel cells were assembled using an identical experimental fuel cell set-up for comparison purposes. The GDLs were compressed to a thickness of 188 μm by using an incompressible polyethylene naphthalate (PEN) gasket, resulting in a compression of 74% (of the original thickness).

Fuel cell operating conditions

A Scribner 850e fuel cell test stand (Scribner Associate Inc., Southern Pines, NC) was used to control the fuel cells by delivering humidified air and hydrogen at an absolute pressure of 200 kPa and a flow rate of 1 standard liter per minute (slpm). The fuel cell operating temperature was maintained at 60°C. Humidified inlet gases were maintained at a dew point of 60°C to achieve an operating relative humidity (RH) of 100%. The high inlet gas RH was chosen to intentionally encourage mass transport limited conditions where liquid water would be expected to accumulate in the GDL. High stoichiometric ratios were used in order to prevent the accumulation of liquid water in the gas flow channels that may have otherwise influenced the accumulation of liquid water in the GDL. These high stoichiometries were used to help isolate the impact of GDL ageing on the GDL liquid water distribution.

The polarization and power density curves for pristine and aged GDLs were obtained at steady state conditions. The fuel cells were held at a constant current and allowed to reach steady state over a period of 5 minutes. The average voltage was obtained by taking the mean voltage over the last 60 seconds of the constant current set point. In addition to these polarization curves, the fuel cells were held at constant current densities for simultaneous in operando synchrotron imaging. Current densities were held constant at 0.5, 1.0, 1.5, and 2.0 A/cm^2 for 15 minutes at each set point. Unless otherwise specified, the operating conditions remained the same between each case, with the fuel cells only differing by the use of either a pristine or aged GDL.

Synchrotron X-ray radiographic imaging

Synchrotron X-ray radiographic imaging was performed at the Biomedical Imaging and Therapy Bending Magnet beamline (05B1-1) located at the Canadian Light Source Inc. (Saskatoon, Canada) (47). Figure 1 is a schematic of the experimental imaging setup for

synchrotron X-ray radiography. The incident X-ray beam was transmitted through the fuel cell and the attenuated X-ray beam was converted to visible light by the scintillator to facilitate detection by the charged-couple device (CCD) camera. The beamline provided a high intensity monochromatic X-ray beam (10^{11} – 10^{15} photons/s · cm^2) (34), which was set to an energy level of 24 keV. A series of absorption radiographic images of the operating fuel cell were captured with the scintillator and a Hamamatsu ORCA Flash 4.0 CCD camera, achieving a pixel resolution of 6.5 µm at 3 seconds exposure per frame. The obtained raw images were composed of 16-bit greyscale pixel arrays, where the brightness of the pixel was correlated to the attenuated X-ray beam intensity. Figures 2a illustrates an example raw image of the customized fuel cell composed of the anode and cathode flow fields, GDLs, and catalyst-coated membrane (CCM). The GDL in the cathode was specifically analyzed to investigate the liquid water distribution.

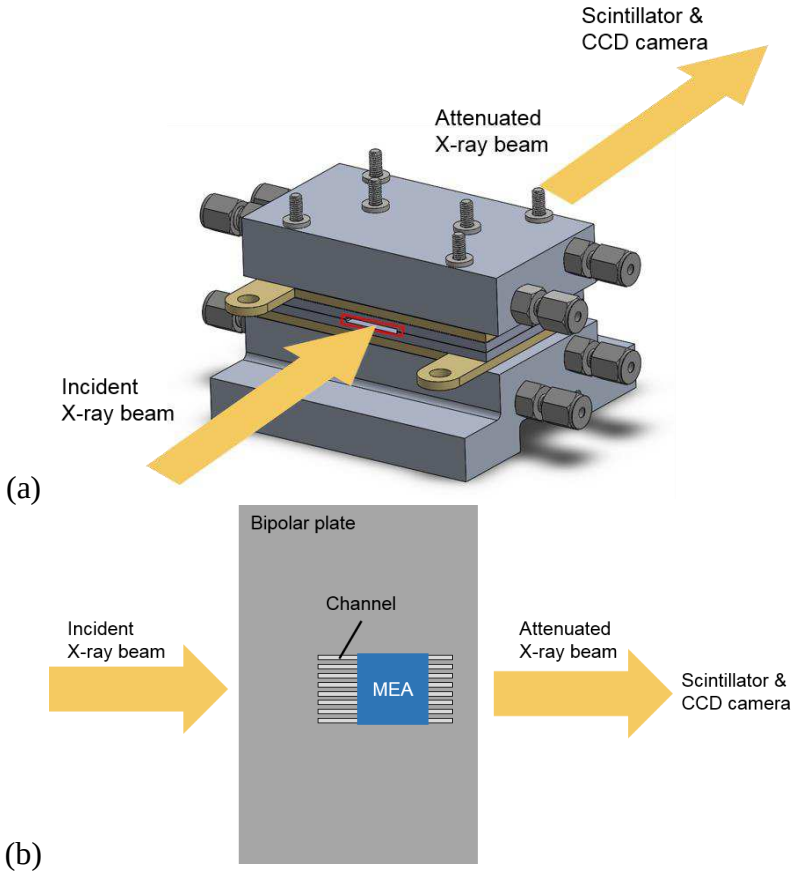

Figure 1. Synchrotron X-ray radiographic imaging experimental setup schematic in a (a) three dimensional view and (b) top view.

Liquid water quantification

The Beer-Lambert law was applied to obtain the liquid water thickness from the obtained radiographic images, as shown in the following (32, 35):

$$I_{wet} = I_{dry} \cdot e^{-\mu_{water} \cdot x_{water}} \quad [1]$$

where x_{water} represents the liquid water thickness [cm], μ_{water} is the X-ray attenuation coefficient of liquid water [cm^{-1}], and I_{wet} and I_{dry} correspond to the pixel intensities of the radiographic image with the presence of liquid water and the reference image with the absence of liquid water [1], respectively. Details of the image processing procedure have been described in our previous work (32, 35).

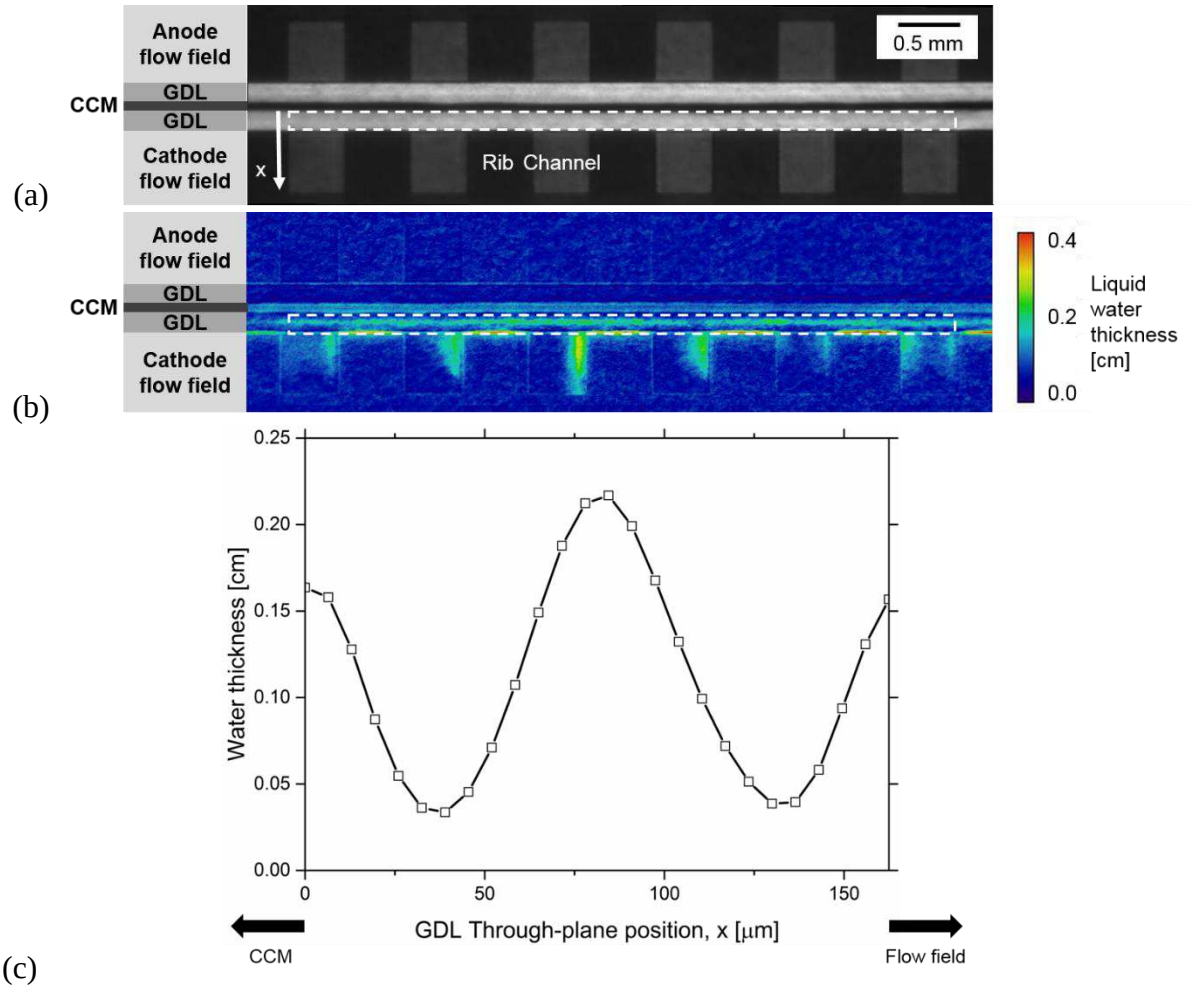

Figure 2. Quantifying liquid water content in a PEM fuel cell from synchrotron in-plane X-ray radiographic imaging: (a) raw image, (b) processed image, and (c) example of liquid water content in the through-plane direction of the selected cathode GDL region. Pixel brightness corresponds to the thickness of liquid water content.

To reduce the inherent noise associated with X-ray radiographic imaging, thirty consecutive frames were averaged to obtain each reported liquid water thickness profile. Figure 2b is an example of a processed image of the fuel cell, where the pixel brightness was directly correlated to the presence of liquid water. Figure 2c is the corresponding cathode liquid water thickness profile with values of liquid water thickness in the through-plane direction obtained by averaging

the in-plane pixel values. In Figure 2c, the through-plane position, *x*, at 0 μm represents the catalyst layer/MPL interface, and the through-plane positon, *x*, at 162.5 μm represents the GDL/flow field interface. The areas of interest that are discussed herein include: the entire GDL, the GDL regions under the channels, and the GDL regions under the ribs. The GDL thickness in the three regions of interest was assumed to be constant since GDL intrusion into the channel was not detected.

Results & Discussion

Ageing effects on overall fuel cell performance

Figure 3 displays the polarization and power density curves acquired for the fuel cell builds with pristine and aged GDLs. At low current densities below 0.5 A/cm^2 (where performance losses were mainly attributed to electrochemical reactions activation losses) pristine and aged GDL fuel cell builds performed almost identically. At intermediate current densities, between 0.5 and 1.0 A/cm^2, slight differences were found between builds. At high current densities above 1.0 A/cm^2, notable performance discrepancies were observed between pristine and aged GDL fuel cell builds. Fuel cells with aged GDLs showed greater performance losses compared to those with pristine GDLs. The trends were also verified by the power density curves. Peak power densities were 0.945 W/cm^2 and 0.720 W/cm^2 for pristine and aged GDL fuel cell builds, respectively. The peak power density output of the fuel cell built with aged GDLs was only 76% of that built with pristine GDLs.

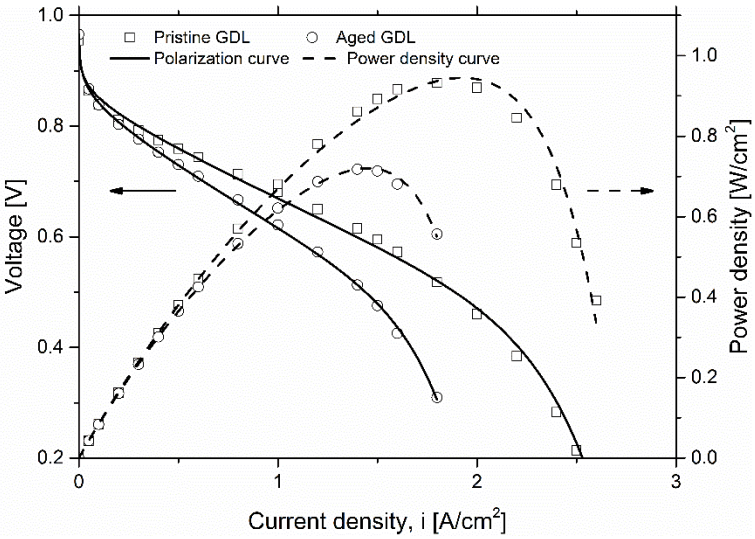

Figure 3. Performance comparison between pristine and aged SGL GDLs.

It was observed that the fuel cell activation loss was independent of GDL ageing. Slight differences in ohmic resistances were due to the differences in PEM hydration between pristine and aged GDL fuel cell builds. Hence, the fuel cell performance difference exhibited in Figure 3 resulted from mass transport resistance differences between pristine and aged GDL fuel cell builds. At higher current densities, large quantities of water were produced at the cathode based on the

cathode electrochemical reaction. Reduced hydrophobicity of the aged GDLs resulted in enhanced GDL flooding, hindering the transport of reactant gases, which led to performance losses. These results are also in agreement with the results that the loss of hydrophobicity led to flooding in the GDL in the literature (2, 6, 16).

Liquid water thickness profile

To explain the differences in mass transport resistances between pristine and aged GDL fuel cell builds, synchrotron X-ray radiographic images were obtained to quantify the accumulation of liquid water in our operating fuel cells. Three areas of interest, including the entire GDL, the GDL regions under the channels, and the GDL regions under the ribs were analyzed to investigate the impacts of ageing. In each area of the GDL, water profiles of region I and II corresponding to the MPL/carbon substrate interfacial region and carbon substrate region, respectively, were identified.

Water content in the entire GDL. Figure 4a and 4b are the cathode liquid water profiles for the entire GDL with pristine and aged GDLs at four current densities: 0.5, 1.0, 1.5 and 2.0 A/cm^2. For both cases, the liquid water profile converged to a final pattern as the current density was incrementally increased. The change in water thickness profiles between pristine and aged GDLs was attributed to the variation of localized porosity distributions between the two materials. We attribute the establishment of a final water profile pattern to the flow field of a distinct liquid water pathway, also known as the breakthrough pattern (48, 49). A breakthrough pattern was established in the aged GDLs at lower current densities compared to that of the pristine GDLs, and this earlier establishment of a breakthrough pattern may be explained by the degradation of hydrophobicity in aged GDLs. Reduction in hydrophobicity would lead to a lower entry capillary pressure. The aged GDL presented lower resistance to liquid water propagation due to these lower entry capillary pressures; therefore, breakthrough patterns were established at lower current densities in contrast to that pristine GDLs.

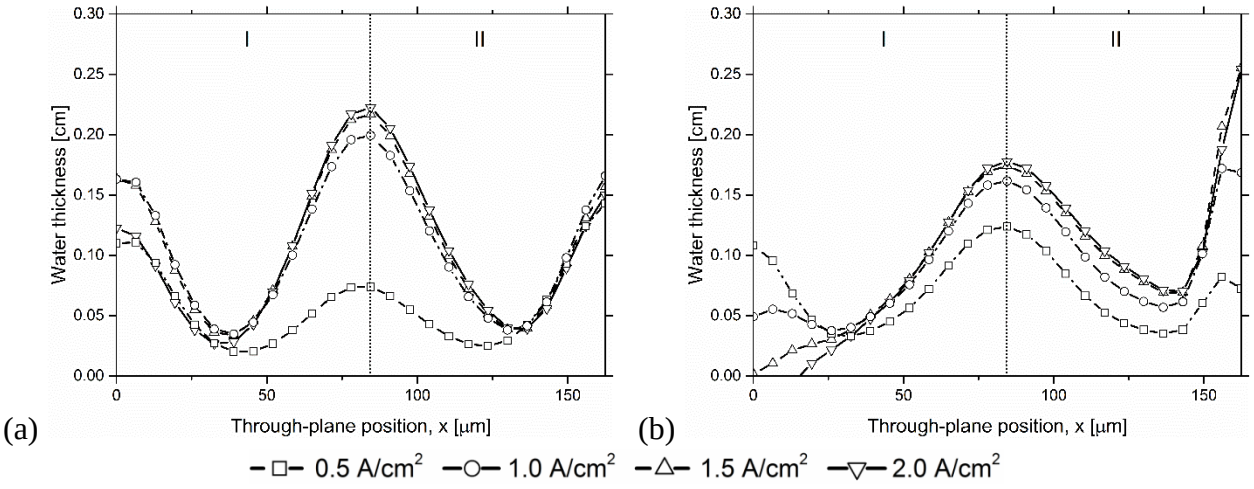

Figure 4. Water content in the entire (a) pristine and (b) aged cathode GDLs at a range of current densities, where I and II are corresponding to the MPL/carbon substrate interfacial region and carbon substrate region, respectively.

An increased quantity of liquid water was also observed at the GDL/flow field interface in aged GDLs. At a current density of 2.0 A/cm^2, the water thickness at the GDL/flow field interface was 0.15 and 0.25 cm for pristine and aged GDLs, respectively. This accumulation of liquid water at the GDL/flow field interface was expected to further hinder the reactant gas from reaching the CL.

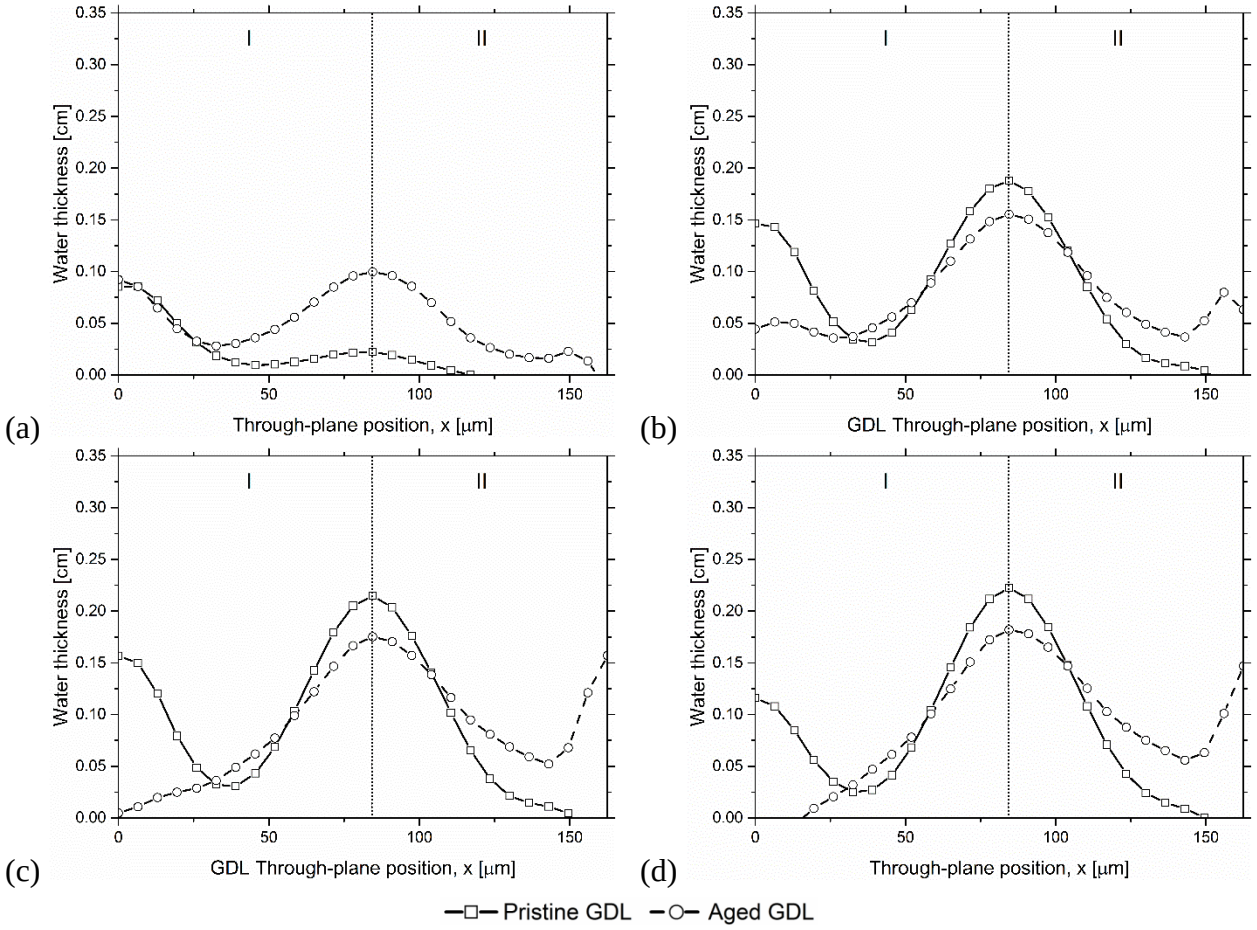

Figure 5. Comparison of cathode liquid water content of pristine and aged materials in areas of the GDL under channels at (a) 0.5, (b) 1.0, (c) 1.5, and (d) 2.0 A/cm^2, where I and II correspond to the MPL/carbon substrate interfacial region and carbon substrate region, respectively.

Water content in areas of the GDL under channels. The water contents in GDLs under the channel and under the rib were studied separately. Figure 5 provides the comparison of cathode liquid water thickness profiles of pristine and aged GDLs under the channel area at various current densities. At a current density of 0.5 A/cm^2 (Figure 5a), significantly more liquid water accumulated in region I and II for aged GDLs. This observation was attributed to the associated loss of hydrophobicity. However, the performance did not vary significantly between the pristine and aged materials as the initial distributions of liquid water did not make a significant impact on the effect transport of reactant gases. At higher current densities of 1.0, 1.5, and 2.0 A/cm^2(Figure 5b – 5c), higher total water contents in region I were observed in pristine GDLs, while region II exhibited higher total water content in aged GDLs. At each current density, the amount of liquid

water produced at the cathode was the same for the aged and pristine GDLs; therefore, changes in liquid water distribution in the GDLs would be expected to have a significant impact on measured fuel cell performance.

In region II, a significantly higher amount of water accumulated at the GDL/channel interface in aged GDLs compared to that of pristine ones. The maximum water thickness in aged GDLs was 0.16 cm, while there was an absence of water at this interface for pristine GDLs. These observations are in agreement with a result obtained through neutron radiography (17, 19). Kätzel and co-workers (17) studied the effects of GDL ageing in an operating fuel cell via neutron radiography. They reported that more liquid water accumulated on the surface of aged GDLs due to the loss to material hydrophobicity. Das et al. (19) reported higher adhesion forces for aged GDLs, which prevented the interfacial water removal with channel gas flow.

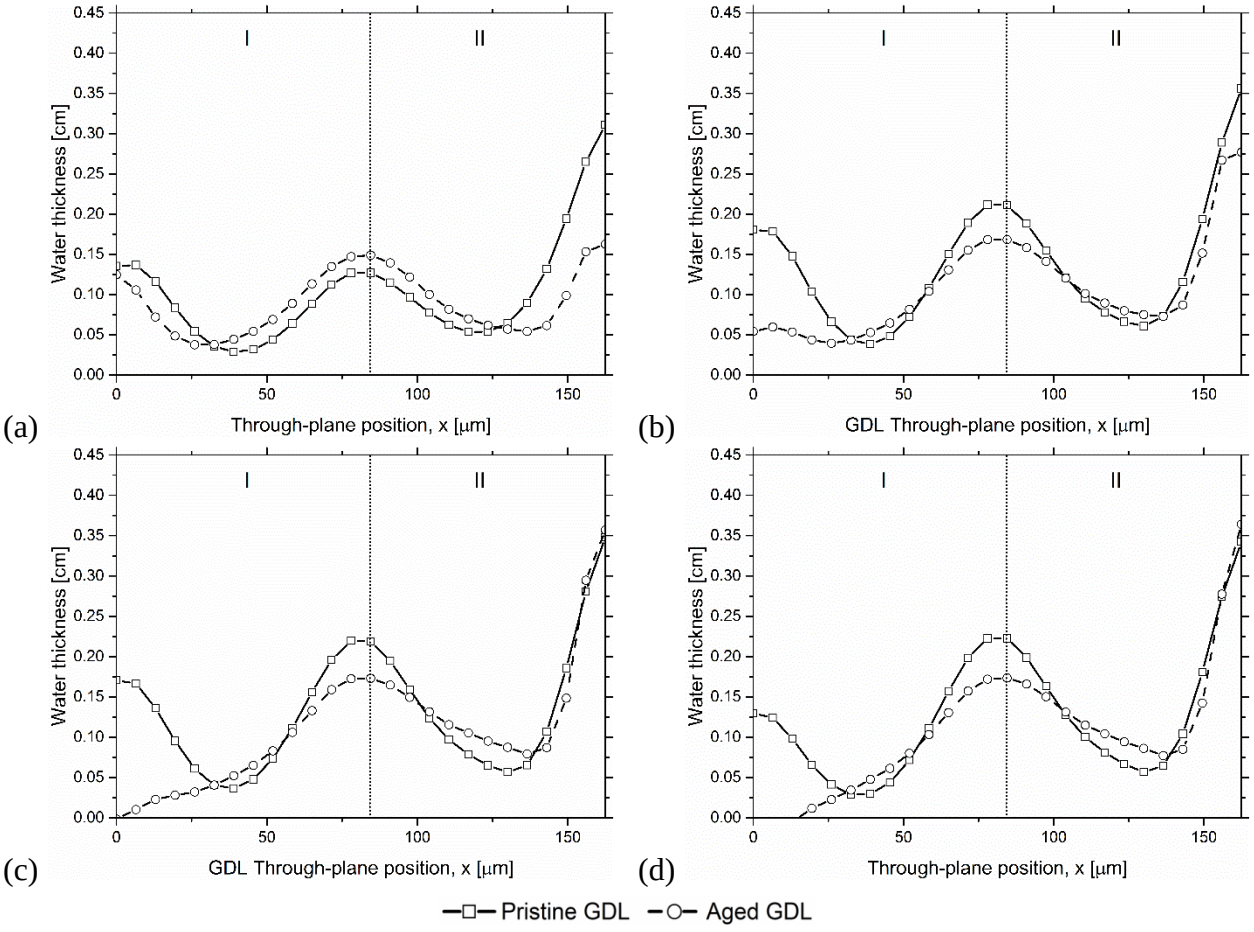

Figure 6. Comparison of cathode liquid water content of pristine and aged materials in areas of the GDL under ribs at (a) 0.5, (b) 1.0, (c) 1.5, and (d) 2.0 A/cm^2, where I and II correspond to the MPL/carbon substrate interfacial region and carbon substrate region, respectively.

Water content in areas of GDLs under ribs. The comparison of cathode liquid water thickness profiles for pristine and aged GDLs under the rib at various current densities was illustrated in

Figure 6. In contrast to Figure 5, similar liquid water thickness results were observed for pristine and aged GDLs. Aged GDLs exhibited greater total liquid water contents at lower current densities, as displayed in Figure 6a; however, these trends were not significant when the current density was increased, as shown in Figures 6b – 6d. Pristine GDLs showed 0.31 cm liquid water content compared to 0.16 cm for aged GDLs at 0.5 A/cm^2 at the GDL/rib interface. At lower current densities of GDL/flow field interface liquid water tended to accumulate in the pristine GDL in contrast to the aged one, and this could be attributed to an additional cooling effect leading to the condensation effect induced in areas of under ribs. However, the water content at the GDL/rib interface did not differ at higher current densities. Therefore, in contrast to the areas of the GDL under channels, the degradation of hydrophobicity had a less significant impact on the areas of the GDL under the ribs.

Conclusions

In this study, synchrotron X-ray radiographic imaging was employed to investigate the impact of GDL ageing on the liquid water transport behavior in an operating fuel cell. As-received pristine GDLs were artificially aged through an accelerated process for 12 hours in-house, and pristine and aged GDLs were used to assemble customized fuel cell builds for in operando synchrotron X-ray radiographic imaging. Performance comparison was also obtained for pristine and aged GDLs fuel cell builds.

It was found that the peak power density of the aged GDL fuel cell build was only 76% of that of the pristine one, and the performance difference was primarily attributed to increases in mass transport resistance. For synchrotron *in situ* visualization results, aged GDLs exhibited higher liquid water contents at low current densities, and breakthrough patterns for aged GDLs converged at lower current density compared to pristine GDLs. Higher quantities of liquid water accumulated at aged GDL/flow field channel interfaces compared to fuel cell builds with pristine GDLs. Higher quantities of liquid water accumulated at the aged GDL/channel interface, and this led to increases in mass transport resistances.

Acknowledgements

The authors acknowledge Dr. George Belev, Dr. Adam Webb, Dr. Ning Zhu and Dr. Tomasz Wysokinski at the Canadian Light Source, in Saskatoon, SK, Canada for their generous assistance. Research described in this work was performed at the Canadian Light Source, which is supported by the Natural Sciences and Engineering Research Council of Canada (NSERC), the National Research Council Canada, the Canadian Institutes of Health Research, the Province of Saskatchewan, Western Economic Diversification Canada, and the University of Saskatchewan. Financial support from the Natural Sciences and Engineering Research Council of Canada, the NSERC Collaborative Research and Training Experience Program (CREATE) Program in Distributed Generation for Remote Communities, the Canada Research Chairs Program, the Ontario Ministry of Research and Innovation Early Researcher Award, and Canadian Foundation of Innovation (CFI) are gratefully acknowledged. Graduate scholarships to Hang Liu from the Connaught International Scholarship for Doctoral Students and the University of Toronto and to

Michael George from NSERC, the Ontario Graduate Scholarship, and the University of Toronto are also gratefully acknowledged.

References

1. Y. Hiramitsu, Y. Hayashi, K. Kobayashi and M. Hori, *Electrical Engineering in Japan.*, **169**, 3 (2009).
2. J. Cho, T. Ha, J. Park, H. Kim, K. Min, E. Lee and J. Jyoung, *Int J Hydrogen Energy.*, **36**, 10 (2011).
3. M. Bosomoiu, G. Tsotridis and T. Bednarek, *J.Power Sources.*, **285** (2015).
4. T. Ha, J. Cho, J. Park, K. Min, H. Kim, E. Lee and J. Jyoung, *Int J Hydrogen Energy.*, **36**, 19 (2011).
5. J. Hu, P. Sui, S. Kumar and N. Djilali, *Electrochim.Acta.*, **54**, 23 (2009).
6. Y. Lee, B. Kim, Y. Kim and X. Li, *Appl.Energy.*, **88**, 12 (2011).
7. Y. Lee, B. Kim, Y. Kim and X. Li, *J.Power Sources.*, **196**, 4 (2011).
8. R. Mukundan, J. R. Davey, K. Rau, D. A. Langlois, D. Spernjak, J. D. Fairweather, K. Artyushkova, R. Schweiss and R. L. Borup, *ECS Transactions.*, **58**, 1 (2013).
9. M. L. Perry, T. Patterson and T. Madden, *ECS Transactions.*, **33**, 1 (2010).
10. S. Yu, X. Li, J. Li, S. Liu, W. Lu, Z. Shao and B. Yi, *Energy Conversion and Management.*, **76** (2013).
11. N. Zamel and X. Li, *Progress in Energy and Combustion Science.*, **37**, 3 (2011).
12. V. Radhakrishnan and P. Haridoss, *Int J Hydrogen Energy.*, **35**, 20 (2010).
13. J. Wu, J. J. Martin, F. P. Orfino, H. Wang, C. Legzdins, X. Yuan and C. Sun, *J.Power Sources.*, **195**, 7 (2010).
14. J. St-Pierre, D. Wilkinsor, S. Knights and M. Bos, *Journal of New Materials for Electrochemical Systems.*, **3**, 2 (2000).
15. K. Seidenberger, F. Wilhelm, T. Schmitt, W. Lehnert and J. Scholta, *J.Power Sources.*, **196**, 12 (2011).
16. S. Kandlikar, M. Garofalo and Z. Lu, *Fuel Cells.*, **11**, 6 (2011).
17. J. Kätzel, H. Markötter, T. Arlt, M. Klages, J. Haußmann, M. Messerschmidt, N. Kardjilov, J. Scholta, J. Banhart and I. Manke, *J.Power Sources.*, **301** (2016).
18. T. Arlt, M. Klages, M. Messserschmidt, H. Riesemeier, J. Scholta, J. Banhart and I. Manke, *ECS Electrochemistry Letters.*, **3**, 2 (2014).
19. P. K. Das, A. Grippin, A. Kwong and A. Z. Weber, *J.Electrochem.Soc.*, **159**, 5 (2012).
20. C. Chen and T. Fuller, *ECS Transactions.*, **11**, 1 (2007).
21. C. Chen and T. F. Fuller, *Electrochim.Acta.*, **54**, 16 (2009).
22. W. Liu and D. Zuckerbrod, *J.Electrochem.Soc.*, **152**, 6 (2005).
23. J. Qiao, M. Saito, K. Hayamizu and T. Okada, *J.Electrochem.Soc.*, **153**, 6 (2006).
24. V. A. Sethuraman, J. W. Weidner, A. T. Haug, S. Motupally and L. V. Protsailo, *J.Electrochem.Soc.*, **155**, 1 (2008).
25. C. Hartnig, I. Manke, R. Kuhn, S. Kleinau, J. Goebbels and J. Banhart, *J.Power Sources.*, **188**, 2 (2009).
26. R. Alink, J. Haussmann, H. Markoetter, M. Schwager, I. Manke and D. Gerteisen, *J.Power Sources.*, **233** (2013).

27. P. Antonacci, S. Chevalier, J. Lee, R. Yip, N. Ge and A. Bazylak, *Int J Hydrogen Energy.*, **40**, 46 (2015).
28. P. Antonacci, S. Chevalier, J. Lee, N. Ge, J. Hinebaugh, R. Yip, Y. Tabuchi, T. Kotaka and A. Bazylak, *Electrochim.Acta.*, **188** (2016).
29. S. Chevalier, N. Ge, J. Lee, P. Antonacci, R. Yip, M. George, H. Liu, R. Banerjee, M. Fazeli and A. Bazylak, *Electrochemistry Communications.*, **59** (2015).
30. J. Eller, J. Roth, F. Marone, M. Stampanoni, A. Wokaun and F. Büchi N., *J.Power Sources.*, **245** (2014).
31. J. Eller and F. N. Buechi, *Journal of Synchrotron Radiation.*, **21** (2014).
32. N. Ge, S. Chevalier, J. Hinebaugh, R. Yip, J. Lee, P. Antonacci, T. Kotaka, Y. Tabuchi and A. Bazylak, *Journal of synchrotron radiation.*, **23**, 2 (2016).
33. J. Haussmann, H. Markoetter, R. Alink, A. Bauder, K. Dittmann, I. Manke and J. Scholta, *J.Power Sources.*, **239** (2013).
34. J. Hinebaugh, P. Challa and A. Bazylak, *Journal of synchrotron radiation.*, **19**, 6 (2012).
35. J. Hinebaugh, J. Lee and A. Bazylak, *J.Electrochem.Soc.*, **159**, 12 (2012).
36. J. Hinebaugh, J. Lee, C. Mascarenhas and A. Bazylak, *Electrochim.Acta.*, **184** (2015).
37. P. Krüger, H. Markötter, J. Haußmann, M. Klages, T. Arlt, J. Banhart, C. Hartnig, I. Manke and J. Scholta, *J.Power Sources.*, **196**, 12 (2011).
38. J. Lee, J. Hinebaugh and A. Bazylak, *J.Power Sources.*, **227** (2013).
39. S. Lee, S. Kim, G. Park and C. Kim, *Int J Hydrogen Energy.*, **35**, 19 (2010).
40. H. Markoetter, R. Alink, J. Haussmann, K. Dittmann, T. Arlt, F. Wieder, C. Toetzke, M. Klages, C. Reiter, H. Riesemeier, J. Scholta, D. Gerteisen, J. Banhart and I. Manke, *Int J Hydrogen Energy.*, **37**, 9 (2012).
41. H. Markoetter, J. Haussmann, R. Alink, C. Toetzke, T. Arlt, M. Klages, H. Riesemeier, J. Scholta, D. Gerteisen, J. Banhart and I. Manke, *Electrochemistry Communications.*, **34** (2013).
42. H. Markoetter, K. Dittrnann, J. Haussmann, R. Alink, D. Gerteisen, H. Riesemeier, J. Scholta, J. Banhart and I. Manke, *Electrochemistry Communications.*, **51** (2015).
43. H. Markötter, I. Manke, P. Krüger, T. Arlt, J. Haußmann, M. Klages, H. Riesemeier, C. Hartnig, J. Scholta and J. Banhart, *Electrochem.Commun.*, **13**, 9 (2011).
44. S. Chevalier, N. Ge, J. Lee, P. Antonacci, R. Yip, M. George, H. Liu, R. Banerjee, M. Fazeli and A. Bazylak, *Electrochemistry Communications.*, **59** (2015).
45. S. Chevalier, J. Lee, N. Ge, R. Yip, P. Antonacci, Y. Tabuchi, T. Kotaka and A. Bazylak, *Electrochim.Acta.*, (2016).
46. J. Lee, R. Yip, P. Antonacci, N. Ge, T. Kotaka, Y. Tabuchi and A. Bazylak, *J.Electrochem.Soc.*, **162**, 7 (2015).
47. T. W. Wysokinski, D. Chapman, G. Adams, M. Renier, P. Suortti and W. Thomlinson, *Nuclear Instruments and Methods in Physics Research Section A: Accelerators, Spectrometers, Detectors and Associated Equipment.*, **582**, 1 (2007).
48. J. Hinebaugh, Z. Fishman and A. Bazylak, *J.Electrochem.Soc.*, **157**, 11 (2010).
49. M. Shahraeeni and M. Hoorfar, *J.Power Sources.*, **196**, 14 (2011).